Ultra-Narrow Faraday Rotation Filter at the Rb D_1 Line

Joanna A. Zielińska[1,2], Federica A. Beduini[1], Nicolas Godbout[3] and Morgan W. Mitchell[1,4,*]

[1] *ICFO-Institut de Ciencies Fotoniques, Mediterranean Technology Park, E-08860 Castelldefels (Barcelona), Spain*
[2] *Instytut Fizyki Doświadczalnej, Uniwersytet Warszawski, PL-00-681 Warszawa, Poland*
[3] *COPL, Département de Génie Physique, École Polytechnique de Montréal, C.P. 6079, Succ. Centre-ville, Montréal (Québec) H3C 3A7, Canada*
[4] *ICREA, Passeig Lluís Companys, 23, E-08010 Barcelona, Spain*
[*] *Corresponding author: morgan.mitchell@icfo.es*

Compiled February 7, 2012

We present a theoretical and experimental study of the ultra-narrow bandwidth Faraday anomalous dispersion optical filter (FADOF) operating at the rubidium D_1 line (795 nm). This atomic line gives better performance than other lines for the main FADOF figures of merit, e.g. simultaneously 71% transmission, 445 MHz bandwidth and 1.2 GHz equivalent noise bandwidth.

OCIS codes: 020.1335, 010.3640

Ultra-narrow bandwidth optical filters are key elements in laser remote sensing (LIDAR), observational astronomy, free-space communications and quantum optics. Relative to conventional interference filters, FADOFs offer high background-rejection, mechanical robustness, imaging capability and high transmission. FADOFs have been developed for several alkali atom resonances – Cs D_2 [1] and $6S_{1/2} \rightarrow 7P_{3/2}$ [2] lines, Rb D_2 line [3, 4], K (three lines) [5], Na D lines [6], and for Ca [7].

We demonstrate a FADOF on the D_1 line of Rb (wavelength 795 nm). This line, efficiently detected with Si detectors, accessible with a variety of laser technologies, and with large hyperfine splittings, is a favorite for coherent and quantum optics with warm atomic vapors. Applications include electromagnetically-induced transparency [8], stopped light [9], optical magnetometry [10, 11], laser oscillators [12], polarization squeezing [13, 14], quantum memory [15] and high-coherence heralded single photons [16, 17].

Here we show that the Rb D_1 line provides superior FADOF performance. We demonstrate a FADOF surpassing other atoms and other Rb transitions for key figures of merit, including peak transmission $T_{\max}$, transmission bandwidth and equivalent noise bandwidth ENBW $= T_{\max}^{-1} \int T(\nu) d\nu$, where $T(\nu)$ is the filter transmission versus frequency ν [4].

A FADOF, shown schematically in Figure 1 (inset), consists of an atomic vapor cell between two crossed polarizers. A homogeneous magnetic field along the propagation direction induces circular birefringence in the vapor. The crossed polarizers block transmission away from the absorption line, while the absorption itself blocks resonant light. Nevertheless, Faraday rotation just outside the Doppler profile can give high transmission for a narrow range of frequencies. FADOF is simple and robust, but performance depends critically on optical properties of the atomic vapor. We model these with a first-principles calculation and find excellent agreement with experiment, as shown in Figure 1.

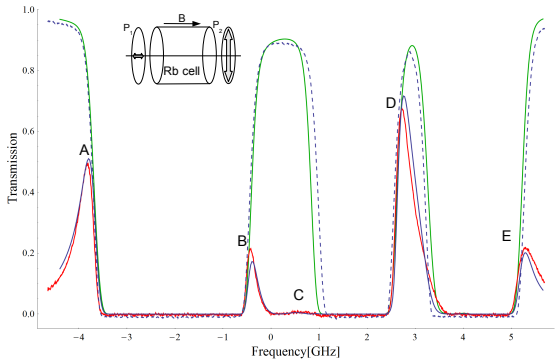

Figure 1. Absorption spectrum for Rb D_1: theory (green), experiment (black dashed). FADOF transmission spectrum: theory (blue), experiment (red). Conditions: $T = 365$ K, $B = 4.5$ mT. Inset - FADOF setup.

Experiment

We use a rubidium cell, with anti-reflection coated windows, a 10 cm internal path, no buffer gas or wall coatings and natural abundance rubidium (Technical Glass, Inc.). An oven and solenoidal field coil allow the cell to be maintained at constant temperature in a uniform axial field. Probe light at 795 nm from a Littrow-configuration external-cavity diode laser (Toptica DL100) is spatially-filtered with a fiber and prepared in an adjustable linear polarization using quarter- and half-waveplates. After the cell, the beam is polarization-filtered with a linear polarizer (colorPol VIS IR) and detected with a low-noise amplified photodiode.

Saturated absorption spectroscopy was used to calibrate field strength produced by the solenoid current, as shown in Figure 2. Labeling the eigenstates by the total angular momentum quantum numbers (F, m_F), the

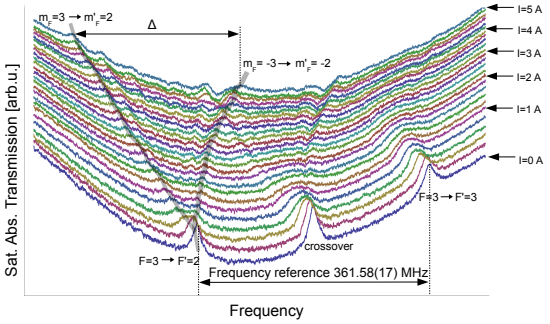

Figure 2. Saturated absorption spectra of the Doppler-broadened line (^{85}Rb transitions from the $F = 3$ ground state) for different coil currents. Splitting Δ between Zeeman-split lines provides a precise measure of the field.

zero-field splitting between the $(3, m) \rightarrow (2, m)'$ and $(3, m) \rightarrow (3, m)'$ transitions of ^{85}Rb provides a precise reference for the frequency scale, while the splitting Δ between $(3, 3) \rightarrow (2, 2)'$ and $(3, -3) \rightarrow (2, -2)'$ is maximally sensitive to magnetic field. Comparing the observed splittings to the first-principles model, we find the field with ± 0.6 % accuracy. Absorption spectra, acquired at the same time as the FADOF spectra, are used to calibrate the frequency axis, which otherwise would be non-linear due to piezo hysteresis. These same spectra indicate the temperature with an uncertainty of $\pm$ 2 K.

The FADOF transmission was measured under a variety of temperature and field conditions in the range T = 355–380 K and B = 3.3–6.0 mT. Typical results, taken at 4.5 mT and 365 K, are shown in Figure 1 and show an agreement with the model at the few-percent level. This field/temperature combination gives a single dominant peak with transmission of 70% at +2.8 GHz relative to line center with FWHM of 445 MHz. Other peaks, of transmission 49%, 17% and 20% are also present, giving an ENBW of 1.2 GHz, considerably better than reported for other atoms. As shown in Table 1, the Rb D_1 FADOF also achieves narrower bandwidths than other transitions and can achieve transmission up to 92% consistent with ultra-low ENBW.

The superior performance of the Rb D_1 line appears to be a fortunate accident of the hyperfine splittings. For either pure ^{85}Rb or pure ^{87}Rb, the FADOF transmission at these field strengths shows four peaks, with the strongest ones at the extremes of the spectrum and with long tails. The strong ^{87}Rb peaks are visible as peak A and E of Figure 1. The strong ^{85}Rb peaks include one at -2.5 GHz, completely obscured by the ^{87}Rb absorption, and the peak D. The long tail of peak D is blocked by absorption from the ^{87}Rb $1 \rightarrow 1$ transition, improving ENBW.

Conclusions

We have demonstrated a Faraday anomalous dispersion optical filter (FADOF) operating at the rubidium D1 line. The filter gives high transmission and narrow bandwidth, with typical numbers being 0.5 GHz bandwidth, maximum transmission of 0.7 and equivalent-noise bandwidth of 1.2 GHz, surpassing similar filters using other atoms and/or other optical transitions. The spectrum can be optimized for different figures of merit by adjusting the temperature and magnetic field conditions of the atomic vapor. A theoretical model shows excellent agreement with experimental results. The simplicity and high noise-rejection may make the new filter attractive for LIDAR and free-space communications and introduces FADOF for the D_1 line, widely preferred for coherent and quantum optical applications.

Table 1. Comparison of reported FADOF transmission for different atoms and wavelengths. T_{max}: peak transmission. B_T: full-width at half-maximum bandwidth of main transmission peak. B_N: Equivalent-noise bandwidth (ENBW). - value not reported. Reference [5] also shows a K 770 nm FADOF curve very similar to K 766 nm.

Atom	λ[nm]	Ref.	T_{max}	B_T[GHz]	B_N[GHz]
K	405	[5]	0.93	1.2	6
Ca	423	[7]	0.55	1.5	-
Cs	455	[2]	0.96	0.9	3.3
Na	589	[6]	0.85	1.9	5.1
Na	590	[6]	0.37	10.5	8.3
K	766	[5]	0.96	0.9	5
Rb	780	[4]	0.93	1.3	4.7
Cs	852	[1]	0.90	0.6	-
T[K]	B[mT]				
353	18.0		0.92	0.48	2.1
378	5.9		0.91	1.10	2.7
365	4.5		0.71	0.45	1.2
345	2.0		0.04	0.32	0.8

Acknowledgements

We thank Y. A. de Icaza Astiz for discussions and assistance. This work was supported by the Spanish Ministry of Science and Innovation under projects FIS2008-01051, FIS2011-27806, and the Consolider-Ingenio 2010 Project "Quantum Optical Information Technologies."

Appendix: FADOF spectra calculation

For completeness, we present the full theoretical model of the Rb D_1 FADOF. A Mathematica notebook to perform the calculations is available with this document at http://arxiv.org/.

The Rb D transitions connect the $5^2S_{J=1/2}$ ground states to the $5^2P_{J=1/2}$ (D_1) and $5^2P_{J=3/2}$ (D_2) excited states. Within each manifold, the Zeeman/hyperfine

structure is determined by the Hamiltonian

$$\begin{aligned}
\hat{H} &= E_{\mathrm{F}} + \hat{H}_{\mathrm{Ze}} + \hat{H}_{\mathrm{HF}} && (1)\\
\hat{H}_{\mathrm{Ze}} &= -g_J\mu_B(\boldsymbol{B}\cdot\hat{\mathbf{J}})\otimes\mathbb{I}_{2I+1} \\
&\quad -g_I\mu_B\mathbb{I}_{2J+1}\otimes(\boldsymbol{B}\cdot\hat{\mathbf{I}}) && (2)\\
\hat{H}_{\mathrm{HF}} &= A_{\mathrm{HF}}\hat{D}_{\mathrm{HF}} + B_{\mathrm{HF}}\hat{Q}_{\mathrm{HF}} && (3)\\
\hat{D}_{\mathrm{HF}} &= \hat{\mathbf{J}}\circ\hat{\boldsymbol{I}} && (4)\\
\hat{Q}_{\mathrm{HF}} &= \begin{cases} \frac{3(\hat{\mathbf{J}}\circ\hat{\boldsymbol{I}})^2+\frac{3}{2}\hat{\mathbf{J}}\circ\hat{\boldsymbol{I}}-I(I+1)J(J+1)}{2I(2I-1)J(2J-1)} & J>1/2 \\ 0 & \text{otherwise}\end{cases} && (5)
\end{aligned}$$

where E_{F} is the level energy including the fine structure contribution, A_{HF} and B_{HF} are magnetic dipole and quadrupole energies, $\hat{\mathbf{J}}$ and $\hat{\mathbf{I}}$ are vector operators representing the total electronic and nuclear angular momenta, respectively, $\hat{\mathbf{J}}\circ\hat{\boldsymbol{I}} \equiv \hat{J}_x\otimes\hat{I}_x + \hat{J}_y\otimes\hat{I}_y + \hat{J}_z\otimes\hat{I}_z$, g_J and g_I are total electronic and nuclear gyromagnetic factors, respectively, $\mathbb{I}_n$ is the n-dimensional identity matrix and μ_B is the Bohr magneton. All constants are taken from Steck [18, 19].

The transition electric dipole operator $\hat{\mathbf{D}}$, with circular components $\hat{D}_q$, $q = 0, \pm 1$, is given by

$$\begin{aligned}
D_q^{J,m_J,J',m'_J} &= \left\langle J||\hat{D}||J'\right\rangle(-1)^{J'-1+m_J} \\
&\quad \times\sqrt{2J+1}\begin{pmatrix} J' & 1 & J \\ m'_J & q & m_J\end{pmatrix} && (6)
\end{aligned}$$

where last expression (:::) is the Wigner 3-j symbol. The reduced dipole moment $\left\langle J||\hat{D}||J'\right\rangle$ for each isotope is given by Steck [18, 19].

For ^{85}Rb ($I = 5/2$) or ^{87}Rb ($I = 3/2$), and for the ground and excited state manifolds, the Hamiltonian of Eq. (1) is diagonalized to find transition frequencies $\omega_{ba} \equiv \omega_b - \omega_a$ and their corresponding dipole matrix elements $D_q^{ab} = \langle a|\,\hat{D}_q\,|b\rangle$, between all pairs of ground and excited states $|a\rangle, |b\rangle$. The (linear) electric susceptibility tensor $\boldsymbol{\chi}$ is diagonal in the circular ($q = \pm 1$) basis, and we compute its diagonal entries (in S.I. units) as

$$\begin{aligned}
\chi_{qq}(\omega) &= \sum_{Z\in\{85,87\}}\frac{N_Z(T)}{\epsilon_0\hbar}\sum_{a,b}|D_q^{ab}|^2(\rho_{bb}-\rho_{aa}) \\
&\quad \times V(\sigma,\frac{\Gamma}{2},\omega_{ba}-\omega) && (7)
\end{aligned}$$

where $N_Z(T)$ is the atomic number density for the isotope Z, T is the temperature, ε_0 is the vacuum permittivity, $\rho \propto \exp[-H/(k_{\mathrm{B}}T)]$ is the atomic density matrix and k_{B} is the Boltzmann constant. The Voigt profile is

$$V(\sigma,\frac{\Gamma}{2},\omega_{ba}-\omega) = i\sqrt{\frac{\pi}{2\sigma^2}}e^{x^2}\mathrm{Erfc}(x), \qquad (8)$$

where Erfc is the complementary error function, $x \equiv [\frac{\Gamma}{2} + i(\omega_{ba}-\omega)]/(\sqrt{2}\sigma)$, and $\sigma = \omega_{ba}\sqrt{k_{\mathrm{B}}T/(M_Z c^2)}$. Atomic masses M_Z and natural linewidths Γ are given in [18, 19].

Atom number density is calculated as $N_Z(T) = c_Z N_Z^{(\mathrm{pure})}(T)$, where c_Z are the relative abundances, the single-isotope densities are $N_Z^{(\mathrm{pure})}(T) = P_Z(T)/(RT)$ where R is the ideal-gas constant and the single-isotope vapor pressures $P_Z(T)$ are from Steck [18,19]. We assume natural abundance $c_{85} = 0.7217$ and $c_{87} = 0.2783$.

The transmission of the filter is

$$T = |E_{\mathrm{det}}^{\dagger}\cdot M_{\mathrm{cell}}\cdot E_{\mathrm{in}}|^2, \qquad (9)$$

where $E_{\mathrm{in}} = (1,1)^T/\sqrt{2}$ is the Jones vector, in the circular left/right basis, of the linearly polarized input, $M_{\mathrm{cell}} = \mathrm{diag}(\exp[in_L kL], \exp[in_R kL])$ is the transmission matrix of the cell, $n_q = \sqrt{1+\chi_{qq}}$, $E_{\mathrm{det}} = (1,-1)/\sqrt{2}$ is the Jones vector of the detected polarization, $k = \omega_{\mathrm{laser}}/c$ and L is the cell internal path length.

References

1. J. Menders, K. Benson, S. H. Bloom, C. S. Liu, and E. Korevaar, Opt. Lett. **16**, 846 (1991).
2. T. Yin, B. Shay, IEEE Photonics Technology Letters **4**, 488 (1992).
3. B. Yin, L. S. Alvarez, and T. M. Shay, "The rb 780-nanometer faraday anomalous dispersion optical filter: Theory and experiment", Tech. rep., Jet Propulsion Laboratory (1994).
4. D. J. Dick and T. M. Shay, Opt. Lett. **16**, 867 (1991).
5. B. Yin and T. Shay, Optics Communications **94**, 30 (1992).
6. H. Chen, C. Y. She, P. Searcy, and E. Korevaar, Opt. Lett. **18**, 1019 (1993).
7. Y. C. Chan and J. Gelbwachs, IEEE Journal of Quantum Electronics **29**, 2379 (1993).
8. X. Yang, S. Li, C. Zhang, and H. Wang, J. Opt. Soc. Am. B **26**, 1423 (2009).
9. R. M. Camacho, P. K. Vudyasetu, and J. C. Howell, Nat Photon **3**, 103 (2009).
10. V. I. Yudin, A. V. Taichenachev, Y. O. Dudin, V. L. Velichansky, A. S. Zibrov, and S. A. Zibrov, Phys. Rev. A **82**, 033807 (2010).
11. F. Wolfgramm, A. Cerè, F. A. Beduini, A. Predojević, M. Koschorreck, and M. W. Mitchell, Phys. Rev. Lett. **105**, 053601 (2010).
12. W. F. Krupke, R. J. Beach, V. K. Kanz, and S. A. Payne, Opt. Lett. **28**, 2336 (2003).
13. J. Ries, B. Brezger, and A. I. Lvovsky, Phys. Rev. A **68**, 025801 (2003).
14. I. H. Agha, G. Messin, and P. Grangier, Opt. Express **18**, 4198 (2010).
15. M. Hosseini, G. Campbell, B. M. Sparkes, P. K. Lam, and B. C. Buchler, Nat Phys **advance online publication**, (2011).
16. A. Cerè, V. Parigi, M. Abad, F. Wolfgramm, A. Predojević, and M. W. Mitchell, Opt. Lett. **34**, 1012 (2009).
17. F. Wolfgramm, Y. A. de Icaza Astiz, F. A. Beduini, A. Cerè, and M. W. Mitchell, Phys. Rev. Lett. **106**, 053602 (2011).
18. D. A. Steck, "Rubidium 85 d line data, revision 2.1.4", available online at http://steck.us/alkalidata (23 December 2010).
19. D. A. Steck, "Rubidium 87 d line data, revision 2.1.4", available online at http://steck.us/alkalidata (23 December 2010).